Next, we illustrate the qualitative relevance of our macroscopic perspective by delineating the meta-narratives of European and North American cultural history, based on birth-death data without additional source material (movies S1 and S2, Fig. 3A, and fig. S14). The sequence of images in Fig. 3A exemplifies the cultural narrative of Europe from 0 to 2012 CE, as presented in movie S1 based on FB: In the beginning, a pan-European elite defined Rome as the center of its empire via massive long-range interactions, followed by increasing point-to-point migration throughout Europe, where Rome remained a hub along with rising subcenters, such as Cordova and Paris. Starting in the 16th century, data density in Europe becomes sufficient to reveal regional clusters. In fact, it becomes evident that Europe is characterized by two radically different cultural regimes: A winner-takes-all regime, with massive centralization toward centers such as Paris, and a fit-gets-richer regime, where many subcenters compete with each other in federal clusters throughout Central Europe and Northern Italy (27) (see Fig. 3, B and C, and fig. S15).

After demonstrating the global quantitative and qualitative relevance of our macroscopic approach, we now focus on the dynamics of individual cultural centers, defined as locations with substantial amounts of notable deaths. We examined notable events identified from the Google Ngram English data set (28), a procedure that can and should be complemented with data sets in other languages to allow for comparison and eventually worldwide coverage (known biases are discussed in the SM). Recording the frequency of words and word combinations in an estimated 5% of all books ever published, the Google Ngram data were originally used to plot the pattern frequency against book publication dates (29). Here, instead, we obtained events by searching for the pattern "{location} in {year}," which allows us to map the "expression" of cultural centers over longer time periods, similar to a gene expression plot (30) (Fig. 4A). Particularly after 1750, dark spikes in the trajectory reveal outstanding historical events. Web searches even allow us to semiautomatically add event labels to these spikes. The resulting Ngram trajectories can be examined relative to total death rate trajectories (Fig. 4B and fig. S16), tracking deviations of locations from their nearly constant fitness $\eta_i^D(t)$ (compare fig. S17 and our model in the SM), and even relative to births and deaths within professional genres in FB, AKL, and ULAN (Fig. 4, C and D). By revealing such correlated changes and continuities, our approach allows for cross-fertilization of domain knowledge into other domains, periods, and geographic areas.

REFERENCES AND NOTES

1. R. L. Carneiro, *The Muse of History and the Science of Culture* (Springer, New York, 2000).
2. L. Spinney, *Nature* **488**, 24–26 (2012).
3. Freebase.com: A community-curated database of well-known people, places, and things (Google, Mountain View, CA, 2011); www.freebase.com.
4. A. Beyer, S. Bénédicte, W. Tegethoff, Eds., *Allgemeines Künstlerlexikon (AKL). Die Bildenden Künstler aller Zeiten und Völker* (De Gruyter, Berlin, 1991, rev. ed. 2010).
5. U. Thieme, F. Becker, Eds., *Allgemeines Lexikon der bildenden Künstler von der Antike bis zur Gegenwart* (Seemann, Leipzig, 1907, rev. ed. 1950).
6. H. Vollmer, Ed., *Allgemeines Lexikon der bildenden Künstler des XX. Jahrhunderts* (Seemann, Leipzig, 1953, rev. eds. 1962 and 1980).
7. Getty Vocabulary Program, *Union List of Artist Names* (The J. Paul Getty Trust, Los Angeles, 2010); www.getty.edu/research/tools/vocabularies/ulan/.
8. Materials and methods are available as supplementary materials on Science Online.
9. G. J. Abel, N. Sander, *Science* **343**, 1520–1522 (2014).
10. N. Keiding, *Philos. Trans. R. Soc.* **332**, 487–509 (1990).
11. Winckelmann-Gesellschaft Stendal, Eds., Corpus der antiken Denkmäler, die J.J. Winckelmann und seine Zeit kannten [database] (Biering & Brinkmann, München, 2000).
12. S. Brin, L. Page, *Comput. Netw. ISDN Syst.* **30**, 107–117 (1998).
13. M. Batty, *Nature* **444**, 592–596 (2006).
14. H. S. Heaps, *Information Retrieval: Computational and Theoretical Aspects* (Academic Press, Waltham, MA, 1978).
15. G. K. Zipf, *Human Behavior and the Principle of Least Effort: An Introduction to Human Ecology* (Addison-Wesley, Boston, 1949).
16. L. M. A. Bettencourt, J. Lobo, D. Helbing, C. Kühnert, G. B. West, *Proc. Natl. Acad. Sci. U.S.A.* **104**, 7301–7306 (2007).
17. L. M. A. Bettencourt, J. Lobo, D. Strumsky, G. B. West, *PLOS ONE* **5**, e13541 (2010).
18. A. Clauset, C. R. Shalizi, M. E. J. Newman, *SIAM Rev.* **51**, 661–703 (2009).
19. E. G. Ravenstein, *J. Stat. Soc. Lond.* **48**, 167–235 (1885).
20. E. G. Ravenstein, *J. R. Stat. Soc.* **52**, 241–305 (1889).
21. G. K. Zipf, *Am. Sociol. Rev.* **11**, 677–686 (1946).
22. P. Ren, *Lifetime Mobility in the United States: 2010* (U.S. Census Bureau, U.S. Department of Commerce, Washington, DC, 2011).
23. D. Brockmann, L. Hufnagel, T. Geisel, *Nature* **439**, 462–465 (2006).
24. C. Song, T. Koren, P. Wang, A.-L. Barabási, *Nat. Phys.* **6**, 818–823 (2010).
25. D. R. White, T. Laurent, N. Kejzar, in *Globalization as Evolutionary Process: Modeling Global Change*, G. Modelski, T. Devezas, W. R. Thompson, Eds. (Routledge, Milton Park, UK, 2007), pp. 190–225.
26. N. Blumm *et al.*, *Phys. Rev. Lett.* **109**, 128701 (2012).
27. G. Bianconi, A.-L. Barabási, *Phys. Rev. Lett.* **86**, 5632–5635 (2001).
28. Google Ngram English data set, version 20090715 (Google, Mountain View, 2009); http://storage.googleapis.com/books/ngrams/books/datasetsv2.html.
29. J.-B. Michel *et al.*, *Science* **331**, 176–182 (2011).
30. M. J. Hawrylycz *et al.*, *Nature* **489**, 391–399 (2012).

DINOSAUR EVOLUTION

Sustained miniaturization and anatomical innovation in the dinosaurian ancestors of birds

Michael S. Y. Lee,[1,2]* Andrea Cau,[3,4] Darren Naish,[5] Gareth J. Dyke[5,6]

Recent discoveries have highlighted the dramatic evolutionary transformation of massive, ground-dwelling theropod dinosaurs into light, volant birds. Here, we apply Bayesian approaches (originally developed for inferring geographic spread and rates of molecular evolution in viruses) in a different context: to infer size changes and rates of anatomical innovation (across up to 1549 skeletal characters) in fossils. These approaches identify two drivers underlying the dinosaur-bird transition. The theropod lineage directly ancestral to birds undergoes sustained miniaturization across 50 million years and at least 12 consecutive branches (internodes) and evolves skeletal adaptations four times faster than other dinosaurs. The distinct, prolonged phase of miniaturization along the bird stem would have facilitated the evolution of many novelties associated with small body size, such as reorientation of body mass, increased aerial ability, and paedomorphic skulls with reduced snouts but enlarged eyes and brains.

The evolution of birds from bipedal carnivorous dinosaurs is one of the most compelling examples of macroevolution (1–7). Numerous studies (1–18) have documented the cumulative evolution of avian characteristics along the ~160 million year (My) lineage leading from large Triassic theropods (oldest widely accepted records, *Herrerasaurus* and *Eodromaeus*, ~230 million years old) to modern birds (Neornithes; oldest widely accepted record,

Vegavis, ~67 million years old). Nevertheless, there remain many intriguing questions regarding size and anatomical evolution along the bird stem lineage. Theropods were typically large to gigantic, but small body size characterized all taxa near the origin of forewing-powered flight in birds [Avialae *sensu* (1–3), Aves *sensu* (15)]. It has been both proposed (4–8) and contested (9–11) that sustained trends of size reduction occurred within theropod evolution. However, most

previous studies of size evolution along the bird stem lineage identified trends anecdotally and used undated cladograms or supertrees, along with parsimony-based character reconstructions [e.g., (4–9, 14)] that ignore vital temporal (branch length) information, which potentially compromise accuracy (19). The only studies to use quantitative likelihood approaches in an explicitly

temporal framework (15, 16) focused on identifying individual branches undergoing fast changes [e.g., Coelurosauria and Paraves (6–8, 15, 16)] and thus did not evaluate directional trends (sustained miniaturization or gigantism) across consecutive branches. Furthermore, rates of anatomical innovation along the bird stem lineage remain underexplored. Most previous studies have evaluated evolutionary rates of a few continuous characters, such as limb proportions or body size (6, 11, 15, 16, 19). However, evolutionary innovation is arguably much better represented by the hundreds of discrete anatomical traits (from across the entire phenotype) that typically make up large phylogenetic data sets.

Here, we identify distinct evolutionary dynamics (sustained miniaturization and accelerated skeletal innovation) in the bird stem lineage, using the most character-rich anatomical data set for dinosaurs compiled to date (20) [data

set 1, expanded from (21): 120 taxa, 1549 skeletal characters, including autapomorphies and invariant characters]. We also analyzed a second matrix (data set 2: 100 taxa, 421 characters) that uses a smaller number of characters but that has been iteratively scrutinized by numerous workers (22), based on (8, 23). Stratigraphic age and femur length were recorded for all adequately known taxa (20). The femur is frequently preserved and scales more tightly with inferred body mass than any other measurement (24) [correlation coefficient $(r) > 0.995$], exhibiting homogenous allometry at least within nonavialan theropods (6). It is thus often used as a size proxy [e.g., (9, 11, 15, 24)] and yields estimates highly consistent with volumetric (14) and composite (16) estimates. Accordingly, we use femur length as a size proxy up to Avialae [but not beyond (6): see supplementary materials (SM), part B]; use of multimeasurement proxies would greatly reduce taxon sampling.

[1]Earth Sciences Section, South Australian Museum, North Terrace, Adelaide 5000, Australia. [2]School of Earth and Environmental Sciences, University of Adelaide 5005, Australia. [3]Museo Geologico e Paleontologico "Giovanni Capellini," Via Zamboni 63, 40126 Bologna, Italy. [4]Dipartimento di Scienze Biologiche, Geologiche e Ambientali, Alma Mater Studiorum Università di Bologna, 40126 Bologna, Italy. [5]Ocean and Earth Science, University of Southampton, Southampton SO14 3ZH, UK. [6]MTA-DE Lendület Behavioural Ecology Research Group, Department of Evolutionary Zoology and Human Biology, University of Debrecen, 4032 Debrecen, Egyetem tér 1, Hungary.
*Corresponding author. E-mail: mike.lee@samuseum.sa.gov.au
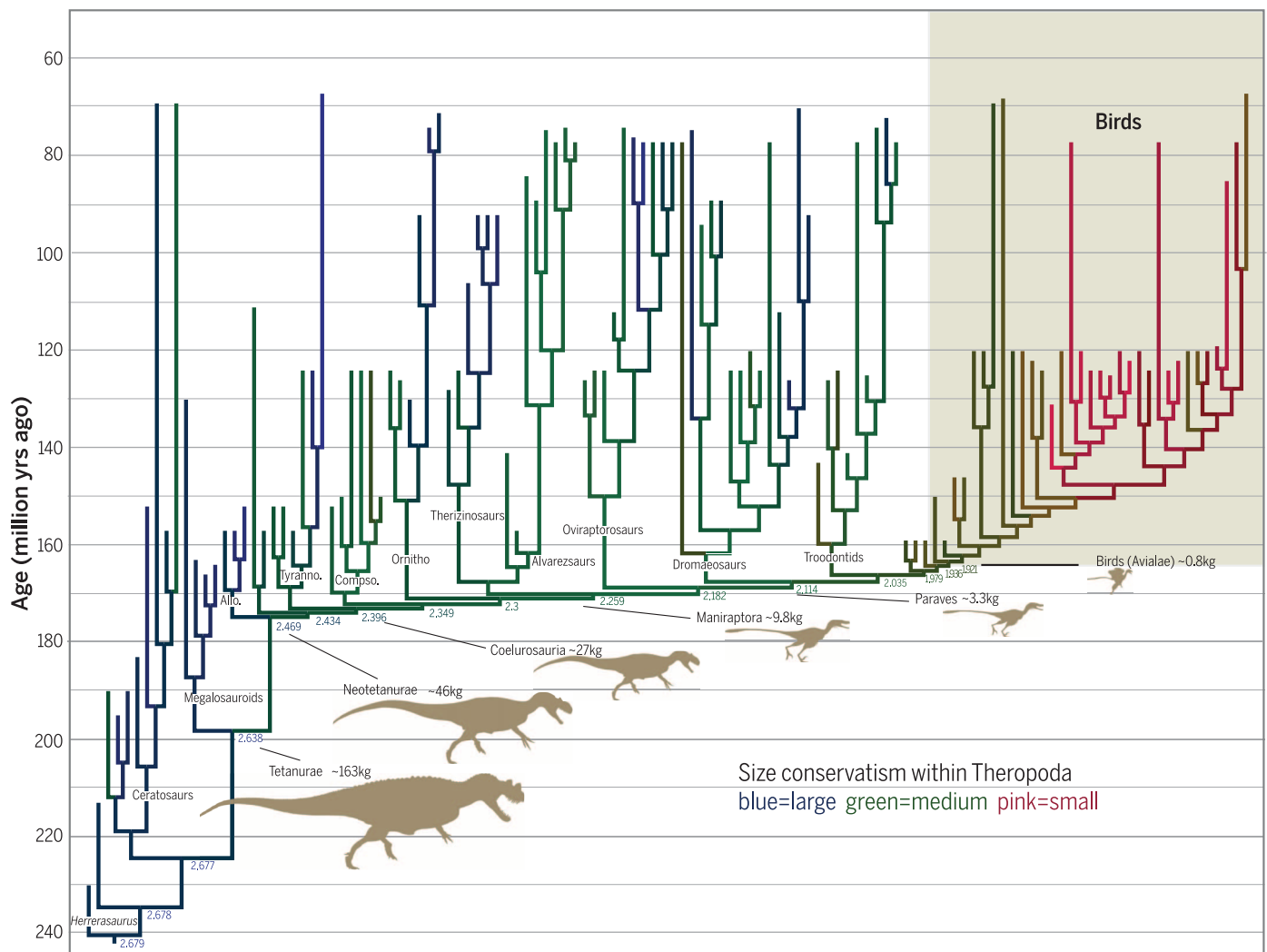
Fig. 1. Body size is highly conserved within theropod dinosaurs; birds and their closest relatives are consistently small. Bayesian maximum clade credibility consensus tree and size reconstructions from data set 1: Branches are colored according to inferred body size (indexed by log$_{10}$ femur length), with ancestral values for nodes along the bird stem lineage shown. All taxon names and size values for all nodes and tips are in fig. S1; posterior probabilities of all clades are in fig. S2. Parsimony analysis reveals similar conservatism (fig. S8), as do Bayesian and parsimony analyses of data set 2 (22, 23) (figs. S5 and S9). Abbreviations: Allo, Allosauroids; Tyranno, Tyrannosauroids; Compso, Compsognathids; Ornitho, Ornithomimosaurs.

The anatomical, stratigraphic, and size data were simultaneously analyzed using Bayesian inference: BEAST (25) modules originally developed for inferring patterns of DNA evolution and geographic spread in "real-time" virus samples were adapted to infer patterns of anatomical evolution and size changes in the "deep-time" fossil record. Bayesian Markov Chain Monte Carlo (MCMC) methods were thus used to reconstruct—with confidence intervals—phylogenetic relations, divergence dates, temporal duration of lineages, evolutionary rates across all 1549 (data set 1) or 421 (data set 2) morphological characters, as well as body size at every ancestral node. This approach explicitly considers the temporal (stratigraphic) distribution of taxa when estimating all these variables. Furthermore, all parameters were simultaneously estimated and thus jointly optimized. Such an approach has been argued to be better for finding global optima and estimating uncertainty (25, 26) and thus preferable to the sequential inference typical of earlier approaches (4–10): inferring topology first, then sometimes inferring divergence dates, and then optimizing the trait of interest. A stochastic Markov model was applied to the discrete character data, with Bayes factors favoring inclusion of parameters for among-trait (gamma) and among-lineage (relaxed clock) rate variation. An undirected Brownian motion model was applied to the continuous (size) data. Tests for directionality using phylogenetic generalized least squares (PGLS) methods [as implemented in BayesTraits (27)] confirmed no significant trends toward size increase or decrease across Theropoda as a whole (9, 10, 28) (SM, part D, and fig. S7), whereas rate-heterogeneous diffusion models proved overparameterized (SM, part C). The significance and robustness of retrieved patterns was corroborated using both (i) simpler parsimony methods for inferring phylogeny and ancestral body sizes (which have been argued to entail fewer assumptions, but are consequently less powerful, and do not adequately measure uncertainty) and (ii) parametric simulations (SM, part E).

Body size, indexed by $\log_{10}$ femur length (FL_{10}), is highly phylogenetically conserved across theropods (Fig. 1 and fig. S1), and there is a prolonged, directional trend in size reduction that spans at least 50 million years and encompasses the entire bird stem lineage from the very base of Theropoda, with rapid decreases in 12 consecutive branches from Tetanurae onward (Fig. 2). The ancestral tetanuran is inferred to be ~198 million years old and ~163 kg, and size then decreases along subsequent nodes as follows; neotetanurans/avetheropods [~174 million years ago (Ma), ~46 kg], coelurosaurs (~173 Ma, ~27 kg), maniraptorans (~170 Ma, ~10 kg), paravians (~167.5 Ma, ~3 kg), and birds (~163 Ma, ~0.8 kg). A similar trend is found for data set 2: FL_{10} again continuously decreases across all bird stem nodes from Tetanurae onward, and there are similar estimated ancestral sizes and divergence dates for each of the above clades (fig. S5). Simulations demonstrate that this trend was sustained across more branches than expected, given a null model of nondirectionality across the entire tree ($P < 0.05$) (SM, part E).

This pervasive trend toward smaller body size along the avian stem lineage is retrieved because the oldest representatives of successively closer outgroups to birds tend to be progressively smaller. The oldest taxon in each outgroup clade tends to be relatively basal and exerts the strongest influence on the reconstructed body size in that part of the bird stem lineage, either because it is separated from the bird stem by chronologically short branch lengths (Bayesian Brownian motion model) or by few intervening nodes (parsimony reconstruction). In this and other studies (Fig. 1 and fig. S5) (3–9, 16, 21, 22), major tetanuran clades branch off the bird stem lineage in this approximate order; megalosauroids, allosauroids, ty-rannosauroids, ornithomimosaurs, alvarezsauroids, oviraptorosaurs, dromaeosaurids, and troodontids. Among the taxa sampled here, the oldest megalosauroid (*Afrovenator*) and allosauroid (*Sinraptor*) with preserved femora are inferred to be ~900 to 1600 kg; the oldest tyrannosauroid (*Guanlong*) and ornithomimosaur (*Harpymimus*) are ~100 kg; the oldest alvarezsauroid (*Haplocheirus*) is ~17 kg; the oldest oviraptorosaur (*Caudipteryx*) is ~5 kg; and the oldest troodontid (*Jinfengopteryx*) and other taxa near the base of birds (Avialae), such as *Archaeopteryx* and *Aurornis*, are consistently ~0.5 kg. Within most outgroup clades, there is concordance between phylogeny and stratigraphy (oldest taxa are generally basal) (Fig. 1); this increases confidence in the phylogenetic results as well as body size reconstructions. Both data sets reveal uncertainty in basal paravian relationships [e.g., (21)]; however, Bayesian MCMC methods, unlike other methods [e.g., (supertrees)], fully integrate over topological and other parameter uncertainty (25, 26).

Our study quantifies rates of evolutionary innovation in dinosaurs using 1549 (data set 1) and 421 (data set 2) skeletal and other anatomical traits distributed across the entire body. A clear pattern emerges: Branches along the bird stem undergo substantially faster morphological evolution than those of the rest of the tree. In data set 1, every branch along the avian stem between Neotetanurae and birds (Fig. 3) evolves at least twice as fast as the average theropod "background" rate: Their average rate of change is 0.0319, which equates to 3.19% divergence per lineage per million years (range 1.96 to 5.33%), approximately four times as fast as the unweighted average branch rate across the entire tree (0.88% per lineage per million years). In both data sets, rates are fastest in the middle region of the bird stem lineage, between the most recent common ancestors of Neotetanurae and Paraves; these peak rates are consistent with
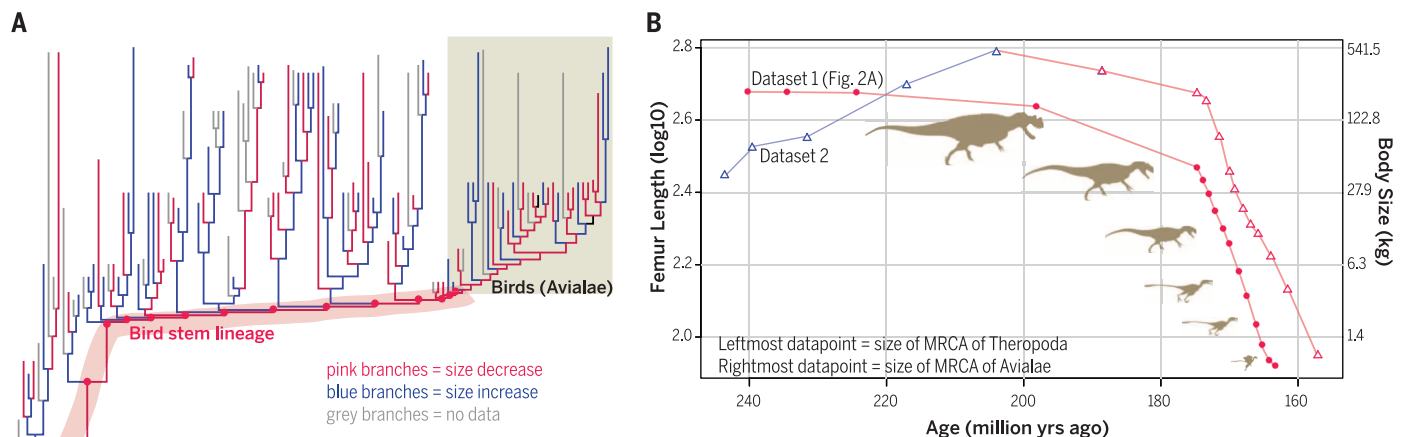
Fig. 2. Sustained miniaturization along the bird stem lineage is distinct among theropod dinosaurs. (**A**) Theropod tree from data set 1 (Fig. 1), with branches color-coded according to whether body size decreases (pink) or increases (blue). Pink branches span basal theropods to birds; in contrast, the rest of the tree shows no comparable "run" of decreases or increases. Parsimony analysis gives consistent results (fig. S8), as do Bayesian and parsimony analyses of data set 2 (22, 23) (figs. S5 and S9). (**B**) Inferred evolution of body size along the bird stem lineage through time. Plot of body size versus age of successive nodes ("ancestors") along the bird stem lineage (from Fig. 1). Femur length is the left scale on y axis; inferred body size (24) is the right scale on y axis. Curves represent results from data sets 1 and 2; both indicate a sustained, unreversed size decrease commencing ~200 million years ago, with the next 12 or more consecutive nodes each smaller than the preceding.
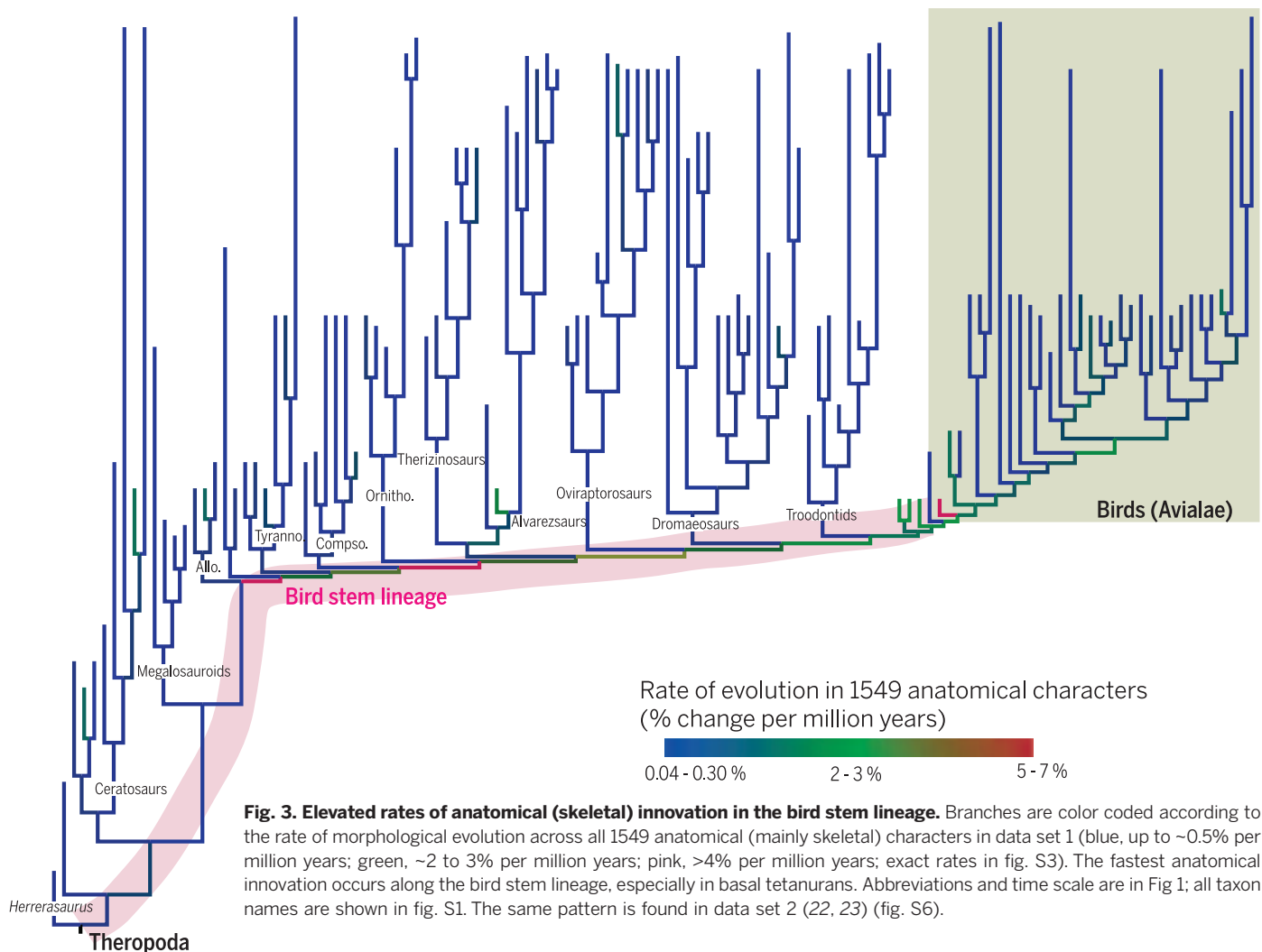
the near-simultaneous stratigraphic appearance (~160 Ma) of several lineages in this part of the tree, notably Allosauroidea, Tyrannosauroidea, Compsognathidae, Alvarezsauroidea, and Paraves. The same patterns are found in data set 2 (fig. S6). The fast-evolving bird stem is not an artifact of internal node age constraints, as it persists in both data sets even if no age constraints (besides root age) are used (SM, part C). However, in such analyses, the peak rates "spread out" onto more basal branches of the bird stem lineage.

Rates of innovation along the bird stem are potentially inflated by oversampling of characters on this lineage (by avian-centric researchers). However, there are three reasons suggesting that the strong rate patterns found here are at least partly real. First, the primary data set (data set 1) attempted to avoid ascertainment bias by explicitly sampling characters across all branches of the theropod tree (including autapomorphies and invariant traits—not sampled in any previous studies). Second, data set 2 was largely constructed to infer relationships among alvarezsaurs (23) and thus likely oversampled characters (and overestimated rates) within this relatively minor

"side" clade, yet nearly all the fastest branches in data set 2 are on the bird stem. Third, Bayesian approaches "dampen" perceived rate heterogeneity by smoothing these patterns when (co)sampling topologies and branch lengths and are thus more conservative in this respect than traditional sequential approaches. Ultimately, the potential effects of character oversampling will best be addressed by independent studies, each aiming to explicitly sample all characters—including autapomorphies and invariant characters—in similar fashion to the collection of molecular sequence data.

These results reconcile contradictory studies identifying presence (4–8) or absence (9–11) of a trend toward size reduction in theropods. Although there is no overall theropod-wide trend (fig. S7 and SM, part D), there is an exceptional trend within the single lineage that comprises much of the avian stem. This prolonged miniaturization is consistent with many aspects of bird origins. Many traits that evolve along the shrinking bird stem lineage are potentially related to developmental truncation, which often accompanies size reduction, regardless of which trait

is under primary selection (29): short snouts, large brains and eyes (12), and smaller teeth with reduced serrations (30). Also, progressive elaboration of feathers along the bird stem, permitting more efficient insulation along with other functions, might have facilitated the evolution of smaller body sizes. Sauropodomorphs (the closest outgroup to theropods) and adequately known basal theropods were entirely or largely featherless; the most basal coelurosaurs had only simple hairlike filaments, whereas ornithomimosaurs and maniraptorans showed a range of more complex feather types (13, 17–19, 21, 22). Finally, the evolution of many avian innovations along the bird stem would have been facilitated by smaller body size, including the reorganization of body mass balance, the increasingly horizontal (and biomechanically demanding) orientation of the femur, a stiffened tail, greater agility and cursoriality, and arboreal and/or aerial habits (1–8, 12–18). Because size reduction, feather elaboration, paedomorphism, and other anatomical novelties permitted by small size all evolved in concert along the bird stem, identifying the primary driver of this sustained trend is probably

Fig. 3. Elevated rates of anatomical (skeletal) innovation in the bird stem lineage. Branches are color coded according to the rate of morphological evolution across all 1549 anatomical (mainly skeletal) characters in data set 1 (blue, up to ~0.5% per million years; green, ~2 to 3% per million years; pink, >4% per million years; exact rates in fig. S3). The fastest anatomical innovation occurs along the bird stem lineage, especially in basal tetanurans. Abbreviations and time scale are in Fig 1; all taxon names are shown in fig. S1. The same pattern is found in data set 2 (22, 23) (fig. S6).

impossible. It is likely that all traits influenced and provided the context for the evolution of others (31).

REFERENCES AND NOTES

1. J. Gauthier, L. F. Gall, Eds., *New Perspectives on the Origin and Early Evolution of Birds* (Peabody Museum of Natural History, New Haven, CT, 2001).
2. G. Dyke, G. Kaiser, Eds., *Living Dinosaurs: the Evolutionary History of Modern Birds* (Wiley, Chichester, UK, 2011).
3. J. Gauthier, *Mem. Calif. Acad. Sci.* **8**, 1–55 (1986).
4. P. C. Sereno, *Annu. Rev. Earth Planet. Sci.* **25**, 435–489 (1997).
5. K. Padian, A. J. de Ricqlès, J. R. Horner, *Nature* **412**, 405–408 (2001).
6. T. A. Dececchi, H. C. E. Larsson, *Evolution* **67**, 2741–2752 (2013).
7. F. E. Novas, M. D. Ezcurra, F. L. Agnolín, D. Pol, R. Ortíz, *Rev. Mus. Argentino de Cienc. Nat. n.s.* **14**, 57–81 (2012).
8. A. H. Turner, D. Pol, J. A. Clarke, G. M. Erickson, M. A. Norell, *Science* **317**, 1378–1381 (2007).
9. M. T. Carrano, in *Amniote Paleobiology*, M. T. Carrano, T. J. Gaudin, R. W. Blob, J. R. Wible, Eds. (Univ. of Chicago Press, Chicago, 2006), chap. 8.
10. D. W. E. Hone, T. M. Keesey, D. Pisani, A. Purvis, *J. Evol. Biol.* **18**, 587–595 (2005).
11. R. B. Sookias, R. J. Butler, R. B. J. Benson, *Proc. Biol. Sci.* **279**, 2180–2187 (2012).
12. B.-A. S. Bhullar *et al.*, *Nature* **487**, 223–226 (2012).
13. A. M. Heers, K. P. Dial, *Trends Ecol. Evol.* **27**, 296–305 (2012).
14. V. Allen, K. T. Bates, Z. Li, J. R. Hutchinson, *Nature* **497**, 104–107 (2013).
15. M. N. Puttick, G. H. Thomas, M. J. Benton, *Evolution* **68**, 1497–1510 (2014).
16. R. B. J. Benson *et al.*, *PLOS Biol.* **12**, e1001853 (2014).
17. D. K. Zelenitsky *et al.*, *Science* **338**, 510–514 (2012).
18. X. Zheng *et al.*, *Science* **339**, 1309–1312 (2013).
19. R. B. J. Benson, J. N. Choiniere, *Proc. Biol. Sci.* **280**, 20131780 (2013).
20. Materials and methods are available as supplementary materials on Science Online. Data files are archived on Dryad Digital Repository (doi:10.5061/dryad.jm6pj).
21. P. Godefroit *et al.*, *Nature* **498**, 359–362 (2013).
22. X. Xu *et al.*, *Nature* **484**, 92–95 (2012).
23. J. N. Choiniere *et al.*, *Science* **327**, 571–574 (2010).
24. P. Christiansen, R. A. Farina, *Hist. Biol.* **16**, 85 (2004).
25. A. J. Drummond, M. A. Suchard, D. Xie, A. Rambaut, *Mol. Biol. Evol.* **29**, 1969–1973 (2012).
26. A. J. Drummond, S. Y. W. Ho, M. J. Phillips, A. Rambaut, *PLOS Biol.* **4**, e88 (2006).
27. M. Pagel, A. Meade, *BayesTraits: Software and Documentation* (2013); www.evolution.reading.ac.uk/BayesTraitsV2Beta.html.
28. L. E. Zanno, P. J. Makovicky, *Proc. Biol. Sci.* **280**, 20122526 (2013).
29. J. Hanken, D. B. Wake, *Annu. Rev. Ecol. Syst.* **24**, 501–519 (1993).
30. O. W. M. Rauhut, C. Foth, H. Tischlinger, M. A. Norell, *Proc. Natl. Acad. Sci. U.S.A.* **109**, 11746–11751 (2012).
31. T. S. Kemp, *Proc. Biol. Sci.* **274**, 1667–1673 (2007).

Digit patterning is controlled by a Bmp-Sox9-Wnt Turing network modulated by morphogen gradients

J. Raspopovic,[1]* L. Marcon,[1]* L. Russo,[1] J. Sharpe[1,2]†

During limb development, digits emerge from the undifferentiated mesenchymal tissue that constitutes the limb bud. It has been proposed that this process is controlled by a self-organizing Turing mechanism, whereby diffusible molecules interact to produce a periodic pattern of digital and interdigital fates. However, the identities of the molecules remain unknown. By combining experiments and modeling, we reveal evidence that a Turing network implemented by Bmp, Sox9, and Wnt drives digit specification. We develop a realistic two-dimensional simulation of digit patterning and show that this network, when modulated by morphogen gradients, recapitulates the expression patterns of *Sox9* in the wild type and in perturbation experiments. Our systems biology approach reveals how a combination of growth, morphogen gradients, and a self-organizing Turing network can achieve robust and reproducible pattern formation.

Digits form in a periodic pattern that alternates digital and interdigital fates along the anterior-posterior (AP) axis of the limb bud. Traditionally, this pattern has been explained by a positional information model (1) based on an AP gradient of Sonic hedgehog (Shh) (2, 3). However, embryonic and genetic manipulations (4, 5) have shown that digit patterning is independent of Shh and may be instead controlled by a self-organizing mechanism. Over three decades ago, it was proposed that such a mechanism could be a Turing system (6, 7), in which a diffusible activator and inhibitor (8) interact and self-organize to form the periodic digit pattern. Recent work has strengthened this hypothesis (9); however, two important questions remain to be addressed.

First, although a number of mathematical Turing models have been proposed to explain the periodic digit pattern (10, 11), no computer simulation has been able to correctly reproduce the expression patterns of digit markers over time and space. Second, the diffusible molecules that implement the Turing network have not yet been identified. Transforming growth factor–β (TGF-β) molecules were proposed as activators in a Turing system (12, 13), but the corresponding diffusible inhibitor could not be found. The galectins CG-1A and CG-8 have also been proposed as Turing molecules in the chick (14) but are not believed to play a similar role in mammals (15). More recently, bone morphogenetic proteins (BMPs) and their receptors have been proposed to form a Turing network (10), but this model assumed that the BMP receptors can diffuse through tissue, for which there is no evidence.

To identify the molecules that control digit specification, it is crucial to distinguish the genes involved in early digit patterning from downstream differentiation factors. We therefore analyzed the expression of the earliest known skeletal marker *Sox9* (16) and identified embryonic day 11.5 (E11.5) as the earliest stage that shows a periodic digital pattern (Fig. 1A). We also performed micromass cultures with E11.5 Sox9-EGFP (enhanced green fluorescent protein) limb autopods (17) and found that cells create a periodic Sox9 pattern by 15 hours, faster than previously reported (18), with dynamics reminiscent of a two-dimensional (2D) Turing simulation (Fig. 1B and movie S1). We observed that the periodic pattern formed even when the culture was initiated with Sox9⁻ or Sox9⁺ cells sorted by fluorescence-activated cell sorting (FACS) (Fig. 1, B and C, and movies S2 and S3), confirming that Sox9 is dynamically regulated by a self-organizing patterning mechanism.

When *Sox9* is knocked out, all the genes that reflect a digital or interdigital pattern (e.g., *Bmp2*, *Chordin*, *Noggin*) lose their normal periodic expression (19), suggesting that *Sox9* itself is part of the Turing network rather than a downstream differentiation marker. The two simplest Gierer-Meinhardt topologies (8), the activator-inhibitor and the substrate-depletion model (Fig. 1D), predict that the diffusible molecules of the Turing network should have periodic patterns that are either in-phase or out-of-phase, respectively. We therefore performed a microarray analysis to identify genes related to the major developmental signaling pathways that were differentially expressed between Sox9⁺ and Sox9⁻ FACS-sorted cells. On the basis of both the number of genes and fold-change magnitude, the pathways that were most strongly represented were WNT, BMP, and FGF (fibroblast growth factor) (fig. S1). We performed a second level of screening by whole-mount in situ hybridization (WMISH) to check which genes were genuinely expressed in-phase

[1]Systems Biology Program, Centre for Genomic Regulation (CRG), and Universitat Pompeu Fabra (UPF), Dr. Aiguader 88, 08003 Barcelona, Spain. [2]Institució Catalana de Recerca i Estudis Avançats (ICREA), Passeig Lluís Companys 23, 08010 Barcelona, Spain.
*These authors contributed equally to this work. †Corresponding author. E-mail: james.sharpe@crg.eu